Long-period incommensurate magnetic orderings associated with the large magnetocaloric effect in $GdCo_2B_2$

Simon Rosenqvist Larsen,* Noriki Terada,† and Hiroaki Mamiya

Research Center for Magnetic and Spintronic Materials, National Institute for Materials Science, 1-2-1, Sengen, Tsukuba, Ibaraki, 305-0047, Japan

Hiraku Saito and Taro Nakajima

Institute for Solid State Physics, The University of Tokyo, 5-1-5 Kashiwanoha, Kashiwa, Chiba Japan 277-8581, Japan

Shinichi Itoh

Institute of Materials Structure Science, High Energy Accelerator Research Organization, 1-1 Oho, Tsukuba, Ibaraki 305-0801, Japan and Materials and Life Science Division, J-PARC Center, 2-4 Shirane Shirakata, Tokai-mura, Naka-gun, Ibaraki 319-1195, Japan

Pascal Manuel, Dmitry Khalyavin, and Fabio Orlandi

ISIS Neutron and Muon Source, Rutherford Appleton Laboratory, Harwell Campus, Didcot, Oxfordshire, OX11 0QX, United Kingdom

Hideaki Kitazawa

Research Center for Energy and Environmental Materials, National Institute for Materials Science, 1-1, Namiki, Tsukuba, Ibaraki, 305-0044, Japan

Abstract

$GdCo_2B_2$ is a member of the $ThCr_2Si_2$ family of compounds which exhibits good magnetocaloric properties associated with antiferromagnetic orderings in the temperature range for hydrogen liquefaction applications. As antiferromagnetic compounds typically do not exhibit a large magnetocaloric effect, understanding the magnetic orderings in $GdCo_2B_2$ could help uncover more magnetocaloric compounds that rely on antiferromagnetic ordering. $GdCo_2B_2$ exhibits four antiferromagnetic phase transitions at 22 K, 18.5 K, 13 K, and 7 K. Due to the difficulty of conducting neutron diffraction measurements on compounds containing affordable natural Gd, the microscopic magnetic structures have so far not been investigated. In this study, by using high energy neutrons and devising special sample preparations for lower energy neutrons, powder neutron diffraction patterns of $GdCo_2B_2$ have successfully been measured. A long-period incommensurate magnetic ordering with $\boldsymbol{k}_1 = (0.0531\ 0\ 0)$ was seen at 20 K. The propagation vector of the incommensurate structure shifted to $\boldsymbol{k}_1 = (0.071\ 0\ 0)$ at 16 K, and an additional $\boldsymbol{k} = (0\ 0\ 0)$ ferromagnetic component was observed. At 10 K two incommensurate propagation vectors of $\boldsymbol{k}_1 = (0.0731\ 0\ 0)$ and $\boldsymbol{k}_2 = (0.0731\ 0.0731\ 0)$, which shifted to $\boldsymbol{k}_1 = (0.0741\ 0\ 0)$ and $\boldsymbol{k}_2 = (0.0741\ 0.0741\ 0)$ at 6 K, were observed to coexist. By considering only the $\boldsymbol{k}_1$-modulation, two possible magnetic structures below 10 K are reported to describe the data, either ac-cycloid structure with constant moment at each Gd site or ellipsoidal ab-cycloid structure. Exchange interaction energy calculations indicated that the long-period antiferromagnetic ordering in $GdCo_2B_2$ is energetically close to the ferromagnetic state due to the strong competition between ferromagnetic and antiferromagnetic exchange interactions, which plays an essential role for the emergence of the large magnetocaloric effect in $GdCo_2B_2$.

I. INTRODUCTION

Driven by the increasing demand for sustainable energy and general cooling, technology based on the magnetocaloric effect has steadily come into prominence. This is due to potential energy efficiency of magnetic refrigeration materials, and the wide temperature range of cooling applications they can be applied to [1]. However, to cover all the different

* larsen.simon@nims.go.jp

† terada.noriki@nims.go.jp

temperature applications a large library of materials is required. Because of this, there are a multitude of physical effects that can contribute to the magnetocaloric properties, and which need to be understood if the materials are to be used.

The magnetic entropy change is currently the main focal point when designing magnetocaloric materials, as its magnitude is one of the main indicators for how effective the material will be at cooling. The magnitude is the largest near the Curie temperature of the material, and therefore the Curie temperature is another major design parameter. In the case of hydrogen liquefaction a temperature region which spans 77 K (temperature of liquid N) to below 20 K is needed. This is a large temperature span and which currently cannot be covered by a single material, and instead an array of materials are necessary. One especially attractive temperature region is around 20 K which is important to avoid hydrogen boil off during storage [2].

The low temperature region of operation has opened up an intriguing possibility for magnetocaloric materials. The main temperature region investigated for applications is for conventional refrigeration around room temperature, where materials with a magnetocaloric effect usually exhibit paramagnetic to ferri- or ferromagnetic structures, with examples such as $La(FeSi)_{13}$ [3], $Gd_5Ge_2Si_2$ [4], and $(Fe,Mn)_2(P,Si)$ [5] being among the most well known. Due to the lower separation of exchange interaction energy in the materials in the temperature region of 20-77 K, many more states become available, significantly broadening the possible magnetic structures that can exhibit magnetic entropy change. In particular, transitions to antiferromagnetic structures become more viable, with the materials showing large entropy changes comparable to the most well-known conventional systems [6] despite the magnetic structure transitions being different from the these. Examples of these materials include Gd_5Ge_4 [7], $ErRu_2Si_2$ [8], Ho_5Pd_2 [9], and the subject of this paper $GdCo_2B_2$ [10]. While the presence of a large entropy change driven by an antiferromagnetic transition in $GdCo_2B_2$ is known, the magnetic structures themselves have not been well studied due to the difficulty in conducting neutron diffraction measurements on compounds containing Gd, which is the most neutron absorbing material in existence.

$GdCo_2B_2$ was first reported in 1973 as a member of the $ThCr_2Si_2$ family of compounds [11]. $ThCr_2Si_2$ is an ordered variant of the $BaAl_4$ structure type, where the $4d$ and $4e$ sites in the tetragonal space group $I4/mmm$ (nr. 139) are occupied by different elements, as can be seen in Fig. 1. The magnetic properties were first investigated in 1984,

which indicated a ferromagnetic ordering below 26 K. The results indicated the moments of the Gd atoms aligned in the basal ab-plane, and that they carried a large moment of 6.4 μ_B [12]. The Co atoms were not found to carry any magnetic moment, which was attributed to the electrons of B filling the conduction band, resulting in the Co atoms being diamagnetic [12, 13].

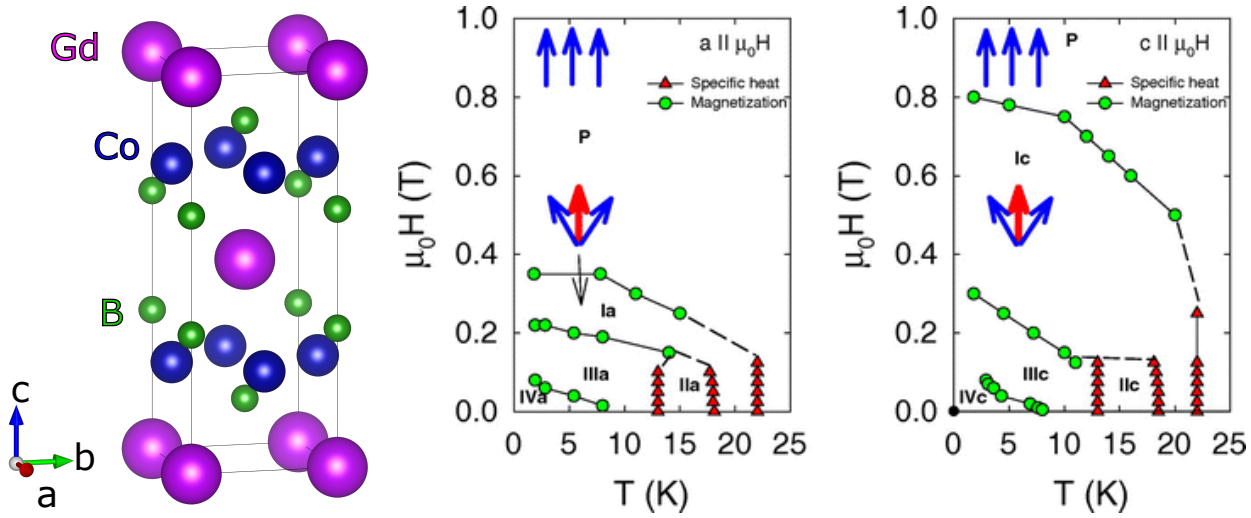

FIG. 1: The unit cell of $GdCo_2B_2$ and the magnetic phase diagram of a single crystal of $GdCo_2B_2$ reported in [14].

In 2009 it was discovered that the system exhibited a reversible giant magnetocaloric effect, the origin of which was attributed to the transition from the newly discovered antiferromagnetic state to the ferromagnetic state [10]. Single crystal magnetization and specific heat measurements confirmed the presence of the antiferromagnetic phases and revealed two additional magnetic transitions in the system, resulting in a total of four transitions observed in $GdCo_2B_2$ [14] as seen in Fig. 1. It was proposed that the system first orders antiferromagnetically at 22 K, and then experiences consecutive transitions to other antiferromagnetic phases at 18.5 K, 13 K and 7 K. In this paper the zero-applied field magnetic phases are named I for 18.5 K $< T <$ 20 K, II for 13 K $< T <$ 18.5 K, III for 7 K $< T <$ 13 K, and IV for $T <$ 7 K in zero applied field. As one of the few antiferromagnetic materials exhibiting a giant magnetocaloric effect, understanding the relationship between the magnetocaloric effect and these magnetic structures is key to finding systems with similar properties for hydrogen liquefaction applications. In this study the magnetic orderings of $GdCo_2B_2$ are studied by neutron powder diffraction.

II. METHODS

Samples of $GdCo_2^{11}B_2$ were synthesized by melting Gd (99.9%), Co (99.99%), and ^{11}B (99.9%) with a molar ratio of 1.05 : 2 : 2 together in an arc-furnace. The resultant button was remelted six times for better homogeneity and then manually ground in a pestle and mortar with acetone as a grinding medium. Powder X-ray diffraction measurements using Cr-radiation did not detect any impurities.

An atom of natural Gd has an absorption cross section of around 49700 b for thermal neutrons with a wavelength of 1.798 Å [15], it is reduced by a factor of around 60 when using high-energy neutrons with a wavelength $\lambda = 0.5$ Å. Because of this, high-energy neutron powder diffraction (NPD) measurements were conducted at the Materials and Life Science Experimental Facility of J-PARC using the beamline BL12 HRC. [16] Powdered $GdCo_2B_2$ was wrapped in a thin layer of Al foil resulting in a packet with a thickness of 1.7 mm. This packet was placed in a sample holder consisting of an Al frame with attachable 25x25 mm^2 front and back windows of V. [17] This was sealed under He atmosphere and the Al edges masked with Cd, and diffraction patterns were measured at temperatures of 37 K, 20 K, 16 K, 10 K and 6 K. The wavelength of $\lambda = 0.565286$ Å was used to measure the diffraction patterns. Due to resonance effects the scattering length of Gd is impacted at this wavelength and it was corrected for by using tabulated values [18].

Due to difficulty assessing the propagation vector of the incommensurate structure, additional measurements were conducted with thermal and cold neutrons (λ = 0.7-10 Å) at the instrument WISH, which is located at the Rutherford Appleton Laboratory at ISIS in Didcot, United Kingdom. [19] To reduce the influence of Gd absorption, particles were sprinkled on varnish (GE7031) on 45x45 mm^2 Al plates. The particles had a size of a few μm, and the thickness of the sample was estimated to be similar to this. [17] The Al plates with sample powder were placed perpendicular to the neutron beam, and measurements were done at temperatures of 40 K, 20 K, 16 K, 10 K, 7 K, and 1.5 K. [20]

III. RESULTS

A. Propagation vectors

The lowest temperature neutron data at 1.5 K in phase IV (measured on WISH) is compared to the paramagnetic data is shown in Fig. 2(a). Here a large magnetic intensity at 0.131 Å^{-1} was observed that could be indexed as *000*$\pm\boldsymbol{k}_1$, signifying a very long period ($\approx$ 48 Å) incommensurate magnetic ordering. Another magnetic satellite reflection was observed at Q close to the *002* reflection with the index *002*$\pm\boldsymbol{k}_1$, as seen in Fig. 2(b). Some other reflections were also observable for Q = 1.75 Å^{-1}, 2.002 Å^{-1}, 2.56 Å^{-1} and 2.74 Å^{-1}, as shown in Figs. 2(c) and 2(d). These reflections could be indexed as listed in Table I, which made it possible to determine the k-vector to be $\boldsymbol{k}_1$ = (0.0741(1) 0 0). It should be noted that an additional reflection at Q = 0.185 Å^{-1} (Fig. 2(a)) was also observed, which could not be indexed by $\boldsymbol{k}_1$. The Q-value of the reflection could be related to that of the magnetic fundamental main reflection at 0.131 Å^{-1} by a factor $\sqrt{2}$. It was possible to index this reflection with the propagation vector $\boldsymbol{k}_2$ = (0.0741(1) 0.0741(1) 0). The two additional reflections observed near the *101* reflection (Fig. 2(c)) could not be indexed, but as they only occurred in one of the diffraction banks and no change in intensity was observed with changing temperatures, it was deemed safe to disregard them.

The temperature of dependence of the magnetic reflections can be seen in Fig. 3. In phase III at 10 K the position of the reflections changed slightly and shifted propagation vectors of $\boldsymbol{k}_1$ = (0.0731(1) 0 0) and $\boldsymbol{k}_2$ = (0.0731(1) 0.0731(1) 0). At the transition temperature of 7 K [17], the propagation vectors were the same as in the 10 K data (Fig. 3(d)), suggesting that a stable region for the propagation vector component might exist before it shifts to the value observed at 1.5 K. While it is possible that the behavior of the propagation vector component relates to the phase transition observed by specific heat measurements at 7 K [14], additional measurements would be needed to verify this. From the present data it is found that the overall microscopic magnetic orderings remain the same between phase IV and III with only a slight change in the propagation vectors.

When the temperature increased to 16 K and phase II was reached, the *000*$\pm\boldsymbol{k}_1$ reflection grew very weak, and the *000*$\pm\boldsymbol{k}_2$ disappeared. A small shoulder on the *002* reflection seen in Fig. 3(b) could be indexed as *002*$\pm\boldsymbol{k}_1$ and indicated that an incommensurate component

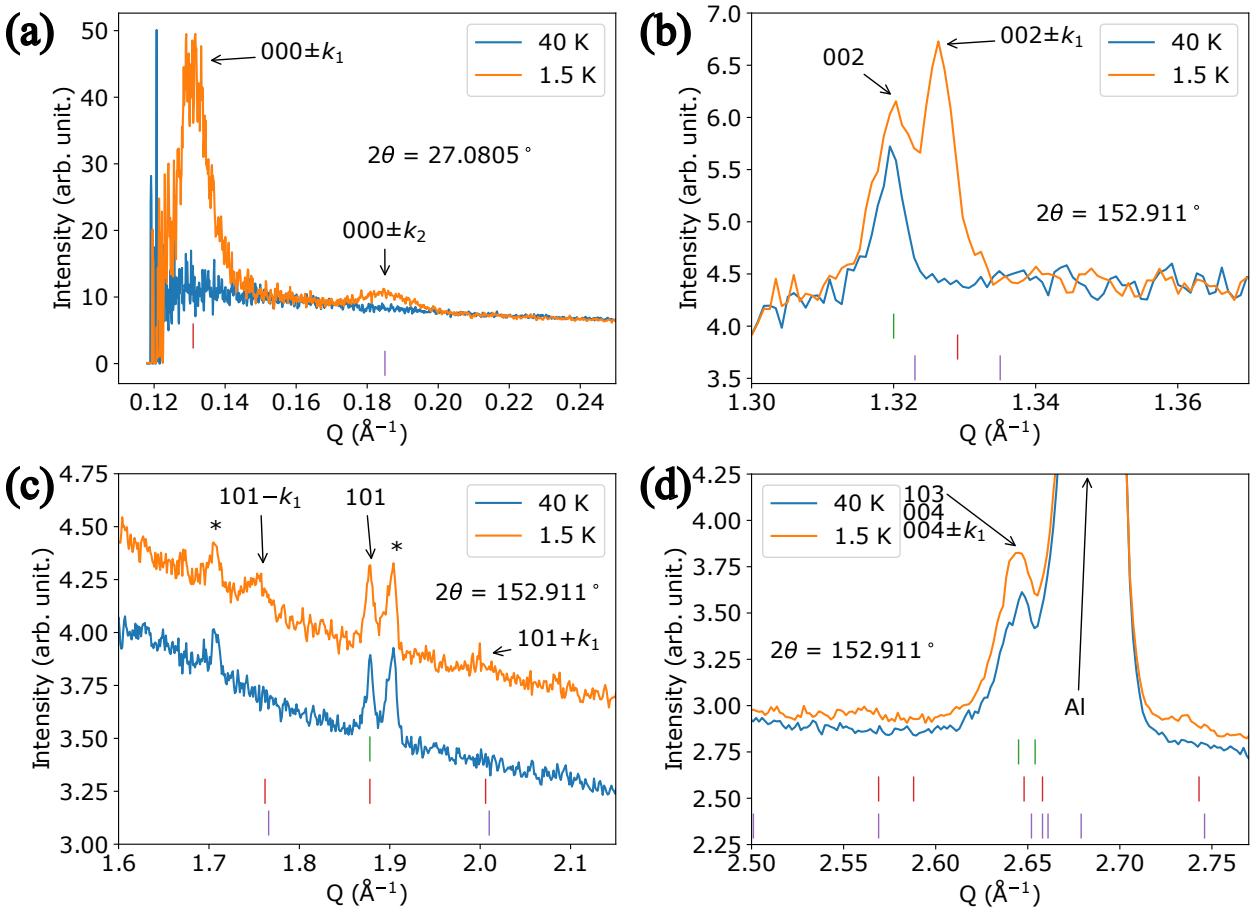

FIG. 2: Diffraction patterns of $GdCo_2B_2$ at 40 K and 1.5 K measured on the WISH beamline. The 2θ positions of the detector banks are stated in the plots, and the patterns have been offset for better readability. The upper line markers refer to the paramagnetic Bragg reflections, the middle line markers refer to the single $\boldsymbol{k}_1 = (0.0741\ 0\ 0)$ component reflections, and the lower line marks refer to the $\boldsymbol{k}_2 = (0.0741\ 0.0741\ 0)$ reflections. The asterisk in (b) denotes reflections associated with an impurity.

still existed. Instead the intensity on the *002* reflection increased, which was consistent with a ferromagnetic ordering with a $\boldsymbol{k} = (0\ 0\ 0)$ propagation vector with moments perpendicular to the c-axis. The $\boldsymbol{k} = (0\ 0\ 0)$ component disappeared in phase I at 20 K leaving only the incommensurate component on the *002*$\pm\boldsymbol{k}_1$ reflection as the magnetic structure contribution and suggesting that only a single propagation vector exists at this temperature. This temperature dependence of the propagation vectors is shown in Fig. 3(d), and presented in Table II.

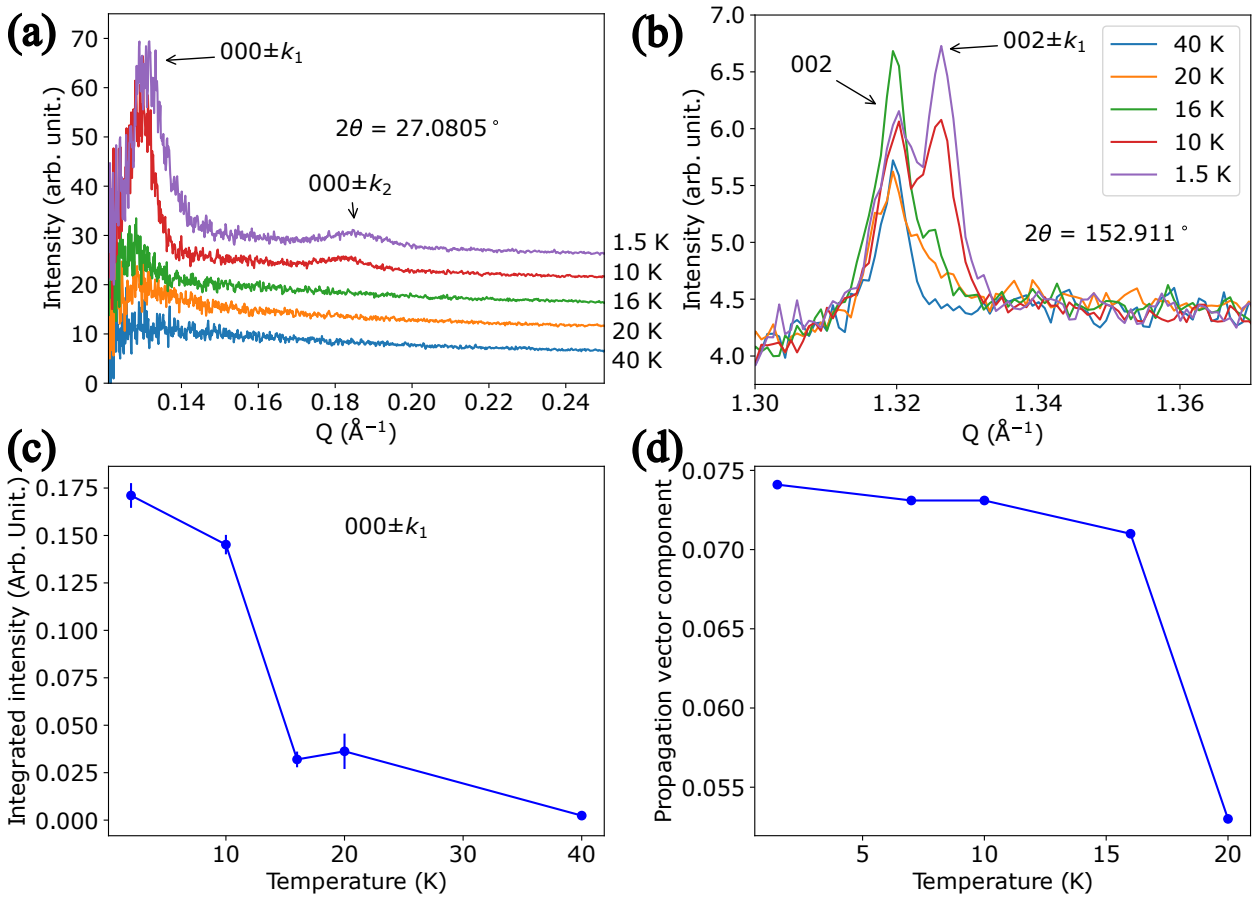

FIG. 3: Evolution of the diffraction patterns due to temperature for (a) the small scattering-angle region, and (b) the *002* reflection. (c) shows the evolution of the integrated intensity of the $000\pm\boldsymbol{k}_1$ reflection. (d) displays the evolution of the propagation vector component with temperature.

B. Structural refinements

While time-of-flight data provided information about the multiple magnetic structures and some propagation vectors, it was of insufficient quality for proper structural model refinements. In order to do proper model refinements, measurements were conducted using high energy neutrons, which would reduce the influence of absorption at the cost of the resolution and access to low scattering angle values.

The crystal structure at the paramagnetic temperature was established from model refinements of data collected at 37 K which are presented in Figure 4, and the extracted parameters of the tetragonal $I4/mmm$ space group can be found in Table II. The model is in line with previous reports on the system with the smaller unit cell parameters being

TABLE I: Observed and calculated positions of incommensurate reflections for $GdCo_2{}^{11}B_2$ at 1.5 K in Q-space. The errors are given in parentheses.

Index	Q_{exp}	Q_{calc}
		$\boldsymbol{k}_1$=(0.0741 0 0)
		$\boldsymbol{k}_2$=(0.0741 0.0741 0)
0 0 0$\pm\boldsymbol{k}_1$	0.131(4)	0.131
0 0 0$\pm\boldsymbol{k}_2$	0.185(6)	0.185
0 0 2$\pm\boldsymbol{k}_1$	1.327(2)	1.329
1 0 1$-\boldsymbol{k}_1$	1.75(1)	1.762
1 0 1$+\boldsymbol{k}_1$	2.002(2)	2.006
1 0 3$-\boldsymbol{k}_1$	2.56(2)	2.569
1 0 3$+\boldsymbol{k}_1$	2.736(2)	2.743
1 1 2$-\boldsymbol{k}_1$		2.743

attributed to the measurement being conducted well below room temperature [10, 14]. The 4*e* site, which hosts the B atoms, is smaller than the $\frac{3}{8}$ typically reported for the $ThCr_2Si_2$ structure type, as well as the 0.371 seen in a previous report on $GdCo_2B_2$. The difference might be caused by the data being measured at different temperatures, and the fact that several of the previous studies do not refine this structural parameter.

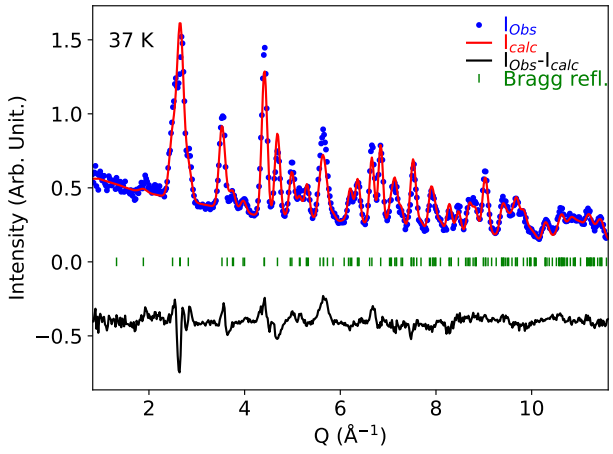

FIG. 4: Model refinements of the neutron powder diffraction data for the paramagnetic state of $GdCo_2B_2$ at 37 K measured at HRC.

TABLE II: Table of refined structural parameters for $GdCo_2{}^{11}B_2$. The errors are given in parentheses.

Measurement	Temp.(K)	a (Å)	c (Å)	4*e* z	Mom. (μ_B)	*k*-vector
HRC	37	3.5632(8)	9.501(3)	0.3500(4)	-	-
	16	3.5653(8)	9.503(3)	0.3500(4)	3.3(2)	-
	10	3.5641(4)	9.503(2)	0.3501(4)	6.6(2)	(0.0731 0 0)
	6	3.5629(4)	9.504(2)	0.3503(4)	6.8(2)	(0.0741 0 0)
WISH	20	3.5639	9.505	0.3507	3.4	(0.053(3) 0 0)
	16	3.5644	9.507	0.3507	5.2	(0 0 0) + ($\approx$ 0.071 0 0)
	10	3.5641	9.501	0.3507	7.4	(0.0731(1) 0 0)
						(0.0731(1) 0.0731(1) 0)
	7	3.5641	9.501	0.3507	7.4	(0.0731(1) 0 0)
						(0.0731(1) 0.0731(1) 0)
	1.5	3.5632	9.501	0.3507	7.4	(0.0741(1) 0 0)
						(0.0741(1) 0.0741(1) 0)

Model refinements of the 20 K data were attempted using a small propagation vector component, but these refinements were highly unstable, likely due to the weak incommensurate component and the lower resolution of the high energy neutron data.

The 16 K data contained a strong ferromagnetic signal permitting stable model refinements using the model with ferromagnetic $\boldsymbol{k}$ = (0 0 0) order and incommensurate $\boldsymbol{k}$ = (0.071 0 0) order. The ferromagnetic moments were found to align in the ab-plane. Although the spin direction could not be determined for the incommensurate component at 16 K due to the weak intensity observed at this temperature, some possibilities can be provided. One possibility of such a structure would be a ferromagnetic component along one of the tetragonal axes in the ab-plane (b-axis in the present case), with a cycloidal structure with spin components in the ac-plane resulting in a conical structure. Another option to consider would be a fan-type magnetic structure with one of the components being parallel to the ferromagnetic moment direction. Model refinements combining the ferromag-

netic structure with the weak incommensurate component were examined to establish which seemed more reasonable. The two models representing a conical structure, and a magnetic fan structure were indistinguishable within the experimental accuracy. Due to the results presented below, an ac-cycloid structure was assumed for the incommensurate component, as this is the same structure seen for 6 K and 10 K. Thus the refinement shown in Fig. 5 depicts a conical structure arising from the combination of the ac-cycloid with a ferromagnetic moment along the b-direction.

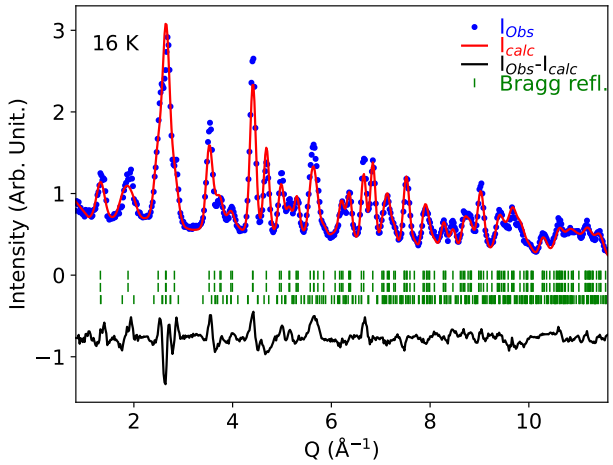

FIG. 5: Model refinements considering a ferromagnetic component along the a-axis, and a weaker ac-cycloid component. Refinements were done on the neutron powder diffraction data for $GdCo_2B_2$ at 16 K measured at HRC.

As with the time-of-flight data, the 10 K (phase III) and 6 K (phase IV) data exhibited much clearer signs of an incommensurate structure, with the *101* reflection at Q $\approx$ 1.8 Å^{-1} showing significant splitting (Fig. 2(c)). Model refinements were done using the propagation vectors, $\boldsymbol{k}_1$ = (0.0741 0 0) and $\boldsymbol{k}_2$ = (0.0741 0.0741 0), attained from the time-of-flight data. While it was possible to conduct the model refinements using both propagation vectors in two separate phases, the contributions from $\boldsymbol{k}_2$ were too small and in many cases overlapped with the $\boldsymbol{k}_1$ propagation vector resulting in no change in the refinement compared to the using only $\boldsymbol{k}_1$. When refining the lowest temperature data (6 K and the lower statistics 10 K) with a single-k model, two possibilities should be considered. One is the case that the Gd moments have a constant length at each site, and the other is the case that the moment length can vary. In general, since Gd 4f moments are localized, only the former case should be considered. However, due to the existence of the $\boldsymbol{k}_2$ component, it is worth considering

the possibility that a multi-k structure exists, and the latter possibility should therefore also be examined. Assuming a constant moment, the ac-cycloid structure best explained the experimental data, as summarized in Fig. 6 and Table III. On the other hand, when allowing for variation in the moment length, the ab-cycloid structure model showed best agreement with the data. This is also consistent with previous magnetization measurements on a single crystal, where the magnetic easy axis was reported to be in the ab-plane. [14] The possibility of a multi-k structure will be discussed in the next section.

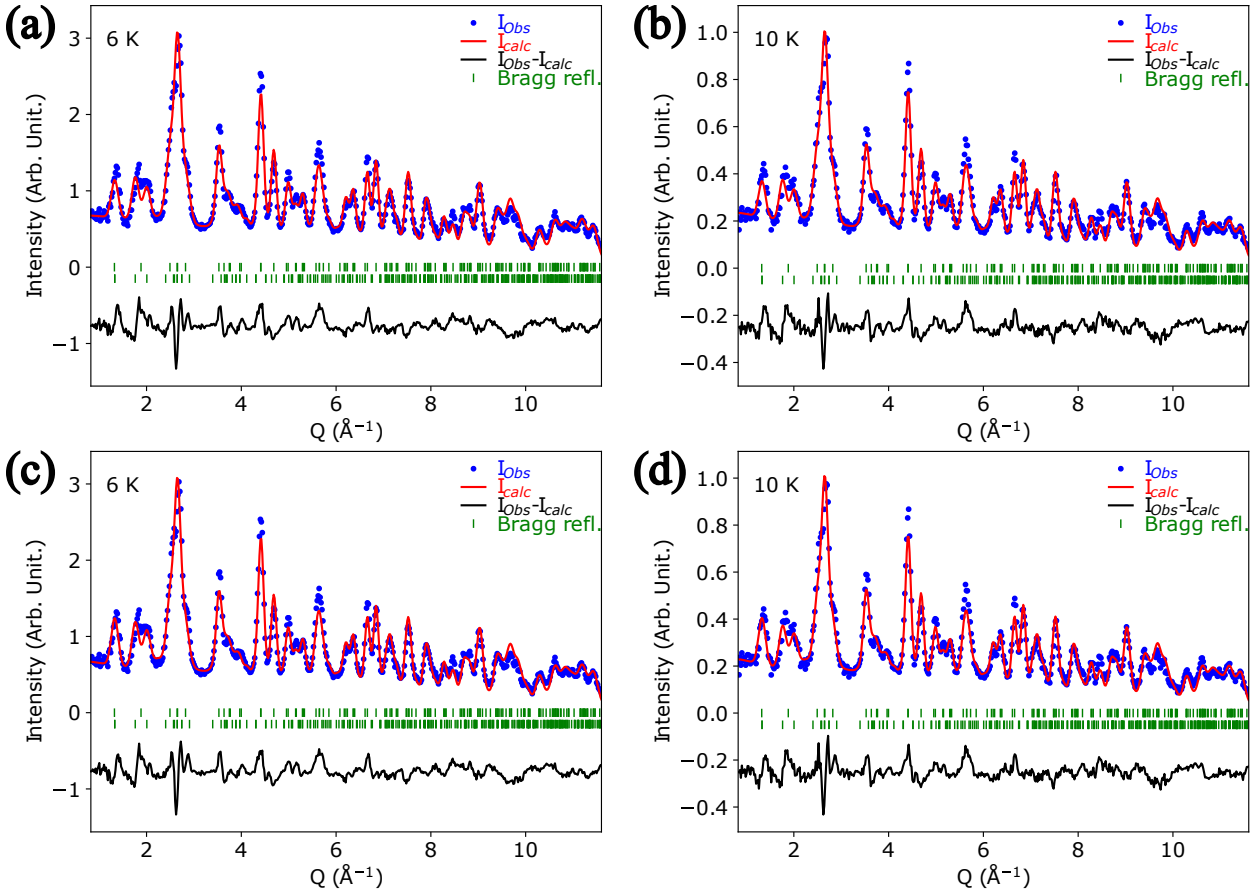

FIG. 6: Model refinements of the neutron powder diffraction data for $GdCo_2B_2$ at 6 K and 10 K. (a) and (b) show the models for an ac-cycloid assuming the same magnetic moment for all Gd sites. (c) and (d) show ab-cycloidal models where the moment in the a- and b-directions are allowed independent components.

TABLE III: Table of tested magnetic structural models of $GdCo_2{}^{11}B_2$. The errors are given in parentheses.

Model type	Moment(μ_B)	R_{Mag}	Moment(μ_B)	R_{Mag}
	10 K		6 K	
ab-cycloid	5.7(2)	11.30	5.8(2)	14.00
ab-cycloid ellipsoidal	$m_a = 4(1)$	9.67	$m_a = 3(1)$	10.90
	$m_b = 6.5(4)$		$m_b = 6.8(4)$	
ac-cycloid	6.6(2)	11.50	6.8(2)	12.70
ac-cycloid ellipsoidal	$m_a = 6.8(4)$	11.20	$m_a = 6.8(4)$	13.00
	$m_c = 6.6(4)$		$m_c = 6.8(3)$	
bc-proper screw	5.2(2)	16.30	5.4(2)	19.10
bc-proper screw ellipsoidal	$m_a = 6.8(4)$	12.40	$m_b = 6.8(4)$	14.60
	$m_c = 2.4(2)$		$m_c = 3(2)$	

IV. DISCUSSION

A. Possibility of multi-k structure

In addition to the main k-vector, $\boldsymbol{k}_1 = (0.0741\ 0\ 0)$, a secondary modulation with $\boldsymbol{k}_2 = (0.0741\ 0.0741\ 0)$ was observed at 10 K and below in phases III and IV. It is not possible to distinguish between a single phase with two k-vectors (multi-k structure), and two phases with different k-vectors (multi domain state) from powder diffraction data. However, it is possible to discuss the likelihood that a multi-k structure exists based on symmetry considerations. In the case of a single phase with two k-vectors, $\boldsymbol{k}_1$ and $\boldsymbol{k}_2$, the latter Fourier component is expected when two arms of the star, $\boldsymbol{k}_1 = (k\ 0\ 0)$ and $\boldsymbol{k}_1\text{'} = (0\ k\ 0)$ are combined (double-k structure), giving rise to the secondary modulation with $\boldsymbol{k}_2 = \boldsymbol{k}_1 + \boldsymbol{k}_1\text{'}$. Time reversal symmetry implies a structural nature of the secondary modulation, unless a ferromagnetic $\boldsymbol{k} = (0\ 0\ 0)$ coexists with $\boldsymbol{k}_1$ and $\boldsymbol{k}_1\text{'}$. In the case of the structural origin of the $\boldsymbol{k}_2$ modulation, it is highly unlikely that such a minuscule distortion can be observed in neutron powder diffraction data, especially when it contains a highly absorbing element such as Gd. The scenario of with the magnetic $\boldsymbol{k}_2$ component requires a spontaneous ferromagnetic

order, which is difficult to determine from the present diffraction data. The larger intensity on the *002* reflection seen for phases III and IV compared to the paramagnetic state and phase I, would seemingly support a multi-k magnetic ordering. However, phases III and IV have much larger intensity on the *002*$\pm\boldsymbol{k}_1$ reflection close to the *002* position, which were not completely separated within the experimental resolution (Fig. 3(b)). It should be noted that magnetization measurements on a single-crystal of $GdCo_2B_2$ reported a net moment in all magnetic states at low applied fields, suggesting that a ferromagnetic moment does indeed exist, which would support the case for a multi-k structure. [14]

The relative success of some of the models considering ellipsoidal magnetic structures presented earlier, could also support the existence of a multi-k structure. It is generally assumed in the case of a single-k structure that the magnetic moments in cycloidal structures are constant when considering the case of localized 4f moments in Gd^{3+}. That the moments in the ab-cycloidal structure vary in the a- and b-directions could be an expression of the differing contributions by $\boldsymbol{k}_1$ and $\boldsymbol{k}_2$ to the overall magnetic structure, resulting in an elliptically shaped moment in the $\boldsymbol{k}_1$-modulation. This would not be the case if $\boldsymbol{k}_1$ and $\boldsymbol{k}_2$ belonged to different domains. It is also possible that the $\boldsymbol{k}_1$+$\boldsymbol{k}_1$**'** component is necessary in order to achieve a constant magnetic moment when combining two elliptical cycloid structures.

The multiple propagation vectors observed are highly reminiscent of other systems known to contain topologically protected structures such as Skyrmions or Merons. This is reasonable given that the largest number of magnetic topological structure compounds have been found in the $ThCr_2Si_2$ structure type [21]. Certain compounds also have astonishingly similar magnetic phase diagrams to that reported for $GdCo_2B_2$ [14] as seen for $EuAl_4$ [22] and $GdRu_2Ge_2$ [23]. The propagation vectors proposed here also show similarity with what was observed in these compounds. The two propagation vectors $\boldsymbol{k}_1$ = (0.0741 0 0) and $\boldsymbol{k}_2$ = (0.0741 0.0741 0) strongly resemble the vectors $\boldsymbol{Q}$ = (0 q 0) and $\boldsymbol{Q}_1$ = (q q 0) which were used to describe a screw structure and square Skyrmion lattice proposed for $EuAl_4$. [22] On the other hand, $\boldsymbol{Q}$ and $\boldsymbol{Q}_1$ were also observed in the zero-field ground state of $EuAl_4$, and resonant X-ray scattering studies revealed that they belonged to distinct magnetic phases. [24] Accordingly, all zero-field spin structures in $EuAl_4$ are single-k. Due to this, considerations of the magnetic structures of $GdCo_2B_2$ have been restricted to the single-k scenario, but considering the above, the possibility of multi-k structures is not excluded, and should be investigated further.

B. Relationship between the large magnetocaloric effect and magnetic orderings

The most commonly used indicator of the magnetocaloric effect is the magnetic entropy ΔS_M when a magnetic field is applied. According to Maxwell's relation $\Delta S_M = \int_0^H \frac{dM}{dT} dH$. Therefore, in ferromagnetic materials, a large magnetization can be induced when a relatively small magnetic field is applied due to the ferromagnetic internal field being added to the external field, resulting in a large ΔS_M. In contrast, for antiferromagnetic materials, the antiferromagnetic exchange interaction energy resists the Zeeman energy induced by the external field. A significant change in magnetization typically does not occur, and a large ΔS_M cannot be expected in antiferromagnets. [25]

In order to understand the relationship between the large magnetocaloric effect and magnetic ordering in $GdCo_2B_2$, the exchange interactions were estimated and examined. Due to the planar behavior of the magnetic structures the calculations were done for a square lattice Heisenberg model considering up to the third next nearest neighbor, in accordance with previous studies concerned with magnetic $ThCr_2Si_2$-based structures [26, 27]. Minimization of energy for the exchange interactions with respect to the propagation vectors produced the phase diagram for the magnetic interactions for the antiferromagnetic nearest neighbor $J_1 < 0$, and ferromagnetic next nearest neighbors $J_2 > 0$ and $J_3 > 0$ (Fig. 7), which is consistent with previously reported phase diagrams. [26, 27] The exchange interactions corresponding to a specific propagation vector for this Heisenberg model can be found using $k_{single} = \arccos(-\frac{J_1+2J_2}{4J_3})$ for $\boldsymbol{k} = (k\ 0\ 0)$ $(J_2 > 2J_3)$, and $k_{double} = \arccos(-\frac{J_1}{2J_2+4J_3})$ for $\boldsymbol{k} = (k\ k\ 0)$ $(2J_3 > J_2)$. Considering the propagation vectors uncovered above, and the simultaneously occurring structures including a ferromagnetic structure, it is likely the that exchange interactions are in the region near the triple point at around $J_2/|J_1| = 0.3$ and $J_3/|J_1| = 0.15$.

In $GdCo_2B_2$, the antiferromagnetic nearest-neighbor exchange interactions and the ferromagnetic second- and third-order exchange interactions can be used to reproduce the k-vector observed in the neutron diffraction data. It is also expected that the competition between these ferromagnetic and antiferromagnetic interactions originating from RKKY interactions [22] can induce a complex sequential phase transition. Although $GdCo_2B_2$ is an antiferromagnet, the exchange energy interactions indicate that the long period magnetic order in the ground state is energetically close a ferromagnetic state. In this situation, since

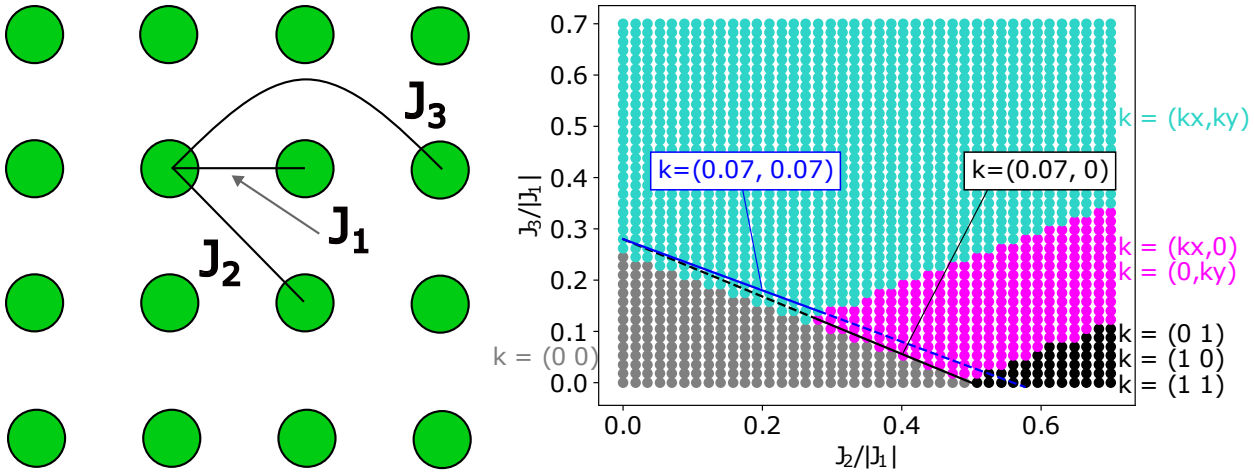

FIG. 7: Heisenberg interactions considered in the square lattice model used to calculate the exchange interaction phase diagram. Lines corresponding to specific propagation vectors are drawn into the phase diagram.

the system has a large magnetic susceptibility in zero field, applying a magnetic field can induce a largely uniform magnetization leading to the large magnetocaloric effect. Indeed, $GdCo_2B_2$ achieves the saturated ferromagnetic state with a magnetic field as low as 0.4 T at the lowest temperature.

C. Comparison to the other $ThCr_2Si_2$type compounds

The magnetic ordering has been studied in many compounds with the $ThCr_2Si_2$ structure type. The vast majority of the members of the rare-earth compound series RCo_2Si_2 and RCo_2Ge_2 are reported to be antiferromagnetic, though R = Y, La, Ce, Lu and Yb did not order and instead exhibited Pauli paramagnetism. In the materials which order the moments align primarily along the c-axis, though the Gd, Er, and Tm based compounds tend to align in the basal plane [28]. Several of these compounds which magnetically order form incommensurate structures, such as $PrCo_2Si_2$ [29], $PrCo_2Ge_2$ [30], $NdCo_2Si_2$ [31], $TbCo_2Si_2$ [32, 33], $DyCo_2Si_2$ [32], $DyCo_2Ge_2$ [33] and $HoCo_2Ge_2$ [33].

In the B based compound $TbCo_2B_2$ the Tb moments align along the c-axis with sinusoidally modulated moment amplitudes with propagation vectors depending on the temperature. From 19 K the propagation vector is the incommensurate $\boldsymbol{k}$ = (0.244 0.244 0) and upon cooling to 10 K reaches commensurability with the vector $\boldsymbol{k}$ = (0.25 0.25 0) [34]. The

moments varied from 2.5 μ_B at 14.1 K to 8.5 μ_B at 1.5 K showing that despite the similarity of the paramagnetic state of the compounds on paper, the behavior of the moments in these compounds is quite different.

Due to the high absorption of Gd there are far fewer reports on compounds based on that element, nevertheless some reports exist on similar compounds. In $GdNi_2Si_2$ an incommensurate structure with a k-vector of $\boldsymbol{k}$ = (0.207 0 0.903) which was described as an amplitude modulated structure with a moment size of 8.05 μ_B, was observed. In the same study $GdCu_2Si_2$ was also investigated, but this compound formed a commensurate antiferromagnetic structure with $\boldsymbol{k}$ = (0.5 0 0.5) and a moment of 7.2 μ_B [35]. In $GdMn_2Si_2$ the Gd moments aligned along the ab-plane and attained a moment size of 6.7 μ_B. With the presence of additional electrons the Mn atoms were also able to align, but did so along the c-axis instead of the ab-plane [36]. $GdCo_2Ge_2$ formed an incommensurate antiferromagnetic structure which aligned in the basal plane of the structure, with a propagation vector of $\boldsymbol{k}$ = (0 0 0.930) [37]. Consequently, in the $ThCr_2Si_2$ structure family of compounds, the strong competition between the RKKY originating exchange interactions results in a large variety of the types of magnetic propagation vectors observed.

V. CONCLUSIONS

Neutron diffraction measurements were conducted on $GdCo_2B_2$ in an effort to uncover the origin of the magnetocaloric effect. In line with previous magnetometric studies, $GdCo_2B_2$ was found to experience four transitions to different magnetic structures. In phase I (18 K $< T <$ 22 K), the magnetic structure was assessed at 20 K, and was found to be an incommensurate structure with a very small propagation vector $\boldsymbol{k}$ = (0.053 0 0). In phase II (12 K $< T <$ 18 K) measured at 16 K, an incommensurate modulation ($\boldsymbol{k}$ = (0.071 0 0)) with a significant ferromagnetic component in the ab-plane was uncovered. Phases III (7 K $< T <$ 12 K) and IV ($T <$ 7 K) did not show clear differences in the diffraction patterns aside from a slight difference in the propagation vector component of the incommensurate structure $\boldsymbol{k}_1 = (k\ 0\ 0)$ with k = 0.0731 for phase III, and k = 0.0741 for phase IV. For phases III and IV, an additional spin modulation ($\boldsymbol{k}_2 = (k\ k\ 0)$), was observed, suggesting that a multi-k structure might exist. From the model refinements considering only $\boldsymbol{k}_1$-modulation, two possible magnetic structures were provided, the first being a ac-cycloid

with constant moments, and the second being an ellipsoidal ab-cycloid. Calculation of the exchange interactions revealed that the observed k-vectors were reproduced by combining an antiferromagnetic nearest-neighbor and ferromagnetic second- and third-neighbor exchange interactions. From the calculations it was found that the long-period antiferromagnetic ordering in $GdCo_2B_2$ is energetically close to the ferromagnetic state and possesses a large magnetic susceptibility near zero field, which plays an essential role for the emergence of significantly large magnetocaloric effect in the antiferromagnet.

ACKNOWLEDGMENTS

The authors would like to thank Ryota Ono and Igor Solovyev for highly useful theoretical calculation discussions. Neutron diffraction measurements conducted at the Materials and Life Science Experimental Facility of the J-PARC was granted through the user program (Proposal numbers 2023A0017 and 2024S0102). Measurements conducted at the ISIS Neutron and Muon Source were done through beamtime RB2420052. This work was supported by JSPS KAKENHI Grant No. 22H00297, and JST-Mirai Program Grant No. JPMJMI18A3 from Japan Science and Technology Agency.

[1] A. Kitanovski. Energy Applications of Magnetocaloric Materials. *Advanced Energy Materials*, 10:1903741, 2020.

[2] S. ZS. Al Ghafri, S. Munro, U. Cardella, T. Funke, W. Notardonato, J.P.M. Trusler, J. Leachman, R. Span, S. Kamiya, G. Pearce, A. Swanger, E.D. Rodriguez, P. Bajada, F. Jiao, K. Peng, A. Siahvashi, M.L. Johns, and E.F. May. Hydrogen liquefaction: a review of the fundamental physics, engineering practice and future opportunities. *Energy & Environmental Science*, 15:2690–2731, 2022.

[3] V. Paul-Boncour and L. Bessais. Tuning the Magnetocaloric Properties of the $La(Fe,Si)_{13}$ Compounds by Chemical Substitution and Light Element Insertion. *Magnetochemistry*, 7:13, 2021.

[4] E. Palacios, J.A. Rodríguez-Velamanzán, G.F. Wang, R. Burriel, G. Cuello, and J. Rodríguez-Carvajal. Magnetic structure of $Gd_5Si_2Ge_2$ and $Gd_5Si_2Ge_{1.9}M_{0.1}$ (M = Ga,Cu). *Journal of*

Physics: Condensed Matter, 22:446003, 2010.

[5] V. Höglin, M. Hudl, L. Caron, P. Beran, M.H. Sørby, P. Nordblad, Y. Andersson, and M. Sahlberg. Detailed study of the ordering in $FeMnP_{0.75}Si_{0.25}$. *Journal of Solid State Chemistry*, 221:240–246, 2015.

[6] V. Franco, J.S. Blázquez, B. Ingale, and A. Conde. The Magnetocaloric Effect and Magnetic Refrigeration Near Room Temperature: Materials and Models. *Annual Review of Materials Research*, 42:305–342, 2012.

[7] A.M.G. Carvalho, A.A. Coelho, S. Gama, P.J. von Ranke, and C.S. Alves. Isothermal variation of the entropy (ΔS_T) for the compound Gd_5Ge_4 under hydrostatic pressure. *Journal of Applied Physics*, 104:063915, 2008.

[8] T. Samanta, I. Das, and S. Banerjee. Giant magnetocaloric effect in antiferromagnetic $ErRu_2Si_2$ compound. *Applied Physics Letters*, 91:152506, 2007.

[9] T. Samanta, I. Das, and S. Banerjee. Magnetocaloric effect in Ho_5Pd_2: Evidence of large cooling power. *Applied Physics Letters*, 91:082511, 2007.

[10] L. Li, K. Nishimura, and H. Yamane. Giant reversible magnetocaloric effect in antiferromagnetic $GdCo_2B_2$ compound. *Applied Physics Letters*, 94:102509, 2009.

[11] K. Niihara, T. Shishido, and S. Yajima. The Crystal Data of Ternary Rare Earth Borides, RCo_2B_2. *Bulletin of the Chemical Society of Japan*, 46:1137–1140, 1973.

[12] I. Felner. Magnetic Properties and Hyperfine Interactions in RCo_2B_2 (R = Nd, Gd, Tb). *Solid State Communications*, 52:191–195, 1984.

[13] R. Ballou, E. Burzo, A. Mincic, and V. Pop. Magnetic properties of $(Gd_xY_{1-x})Co_2B_2$ compounds. *Journal of Magnetism and Magnetic Materials*, 118:L285–L289, 1993.

[14] J. Pospíšil, H. Kitazawa, A. Gupta, S. Toyoizumi, A. Tamaki, M. Diviš, and V. Sechovský. Magnetism in $GdCo_2B_2$ Studied on a Single Crystal. *Journal of the Physical Society of Japan*, 83:054713, 2014.

[15] V.F. Sears. Neutron scattering lengths and cross sections. *Neutron News*, 3:26–37, 1992.

[16] S. Itoh, T. Yokoo, S. Satoh, S. Yano, D. Kawana, J. Suzuki, and T.J. Sato. High Resolution Chopper Spectrometer (HRC) at J-PARC. *Nuclear Instruments and Methods in Physics Research Section A: Accelerators, Spectrometers, Detectors and Associated Equipment*, 631:90–97, 2011.

[17] See Supplemental Material for additional information relating to sample preparation, propagation vector determination, and model refinements.

[18] J.E. Lynn and P.A. Seeger. Resonance Effects in Neutron Scattering Lengths of Rare-Earth Nuclides. *Atomic Data and Nuclear Data Tables*, 44:191–207, 1990.

[19] L.C. Chapon, P. Manuel, P.G. Radaelli, C. Benson, L. Perrott, S. Ansell, N.J. Rhodes, D. Raspino, D. Duxbury, and J. Norris. Wish: The New Powder and Single Crystal Magnetic Diffractometer on the Second Target Station. *Neutron News*, 22:22–25, 2011.

[20] S.R. Larsen, N. Terada, and P. Manuel. Investigation of incommensurate structures in $GdCo_2B_2$, 2025.

[21] T. Nomoto and R. Arita. *Ab initio* exploration of short-pitch skyrmion material: Role of Orbital frustration. *Journal of Applied Physics*, 133:150901, 2023.

[22] R. Takagi, N. Matsuyama, V. Ukleev, L. Yu, J.S. White, S. Francoual, J.R.L. Mardegan, S. Hayami, H. Saito, K. Kaneko, K. Ohishi, Y. Onuki, T. Arima, Y. Tokura, T. Nakajima, and S. Seki. Square and rhombic lattice of magnetic skyrmions in a centrosymmetric binary compound. *Nature Communications*, 13:1472, 2022.

[23] H. Yoshimochi, R. Takagi, J. Ju, N.D. Khanh, H. Saito, H. Sagayama, H. Nakao, S. Itoh, Y. Tokura, T. Arima, S. Hayami, T. Nakajima, and S. Seki. Multistep topological transition among meron and skyrmion crystals in a centrosymmetric magnet. *Nature Physics*, 20:1001–1008, 2024.

[24] A.M. Vibhakar, D.D. Khalyavin, F. Orlandi, J.M. Moya, S. Lei, E. Morosan, and A. Bombardi. Spontaneous reversal of spin chirality and competing phases in the topological magnet $EuAl_4$. *Communications Physics*, 7:313, 2024.

[25] R. Tamura, T. Ohno, and H. Kitazawa. A generalized magnetic refrigeration scheme. *Applied Physics Letters*, 104:052415, 2014.

[26] Z. Wang, Y. Su, S. Lin, and C.D. Batista. Meron, skyrmion, and vortex crystal in centrosymmetric tetragonal magnets. *Physical Review B*, 103:104408, 2021.

[27] M. Gen, R. Takagi, Y. Watanabe, S. Kitou, H. Sagayama, N. Matsuyama, Y. Kohama, A. Ikeda, Y. $\bar{\text{O}}$nuki, T. Kurumaji, T. Arima, and S. Seki. Rhombic skyrmion lattice coupled with orthorhombic structural distortion in $EuAl_4$. *Physical Review B*, 107:L020410, 2023.

[28] A. Szytuła and J. Leciejewicz. Chapter 83 Magnetic properties of ternary intermetallic compounds of the RT_2X_2 type. *Handbook on the Physics and Chemistry of Rare Earths*, 12:133–

211, 1989.

[29] T. Shigeoka, N. Iwata, Y. Hasimoto, Y. Andoh, and H. Fujii. Neutron diffraction studies of $PrCo_2Si_2$ single crystal. *Physica B: Condensed Matter*, 156-157:741–743, 1989.

[30] A. Szytuła, J. Leciejewicz, and H. Bińczycka. Crystal and Magnetic Structures of $PrCo_2Ge_2$ and $HoCo_2Ge_2$. *physica status solidi (a)*, 58:67–70, 1980.

[31] T. Shigeoka, N. Iwata, Y. Hashimoto, Y. Andoh, and H. Fujii. Antiferromagnetic Phases in $NdCo_2Si_2$. *Journal de Physique Colliques*, 49:C8–431–C8–432, 1988.

[32] A. Szytuła, M. Balanda, B. Penc, and M. Hofmann. Neutron study of magnetic phase transitions in $TbCo_2Si_2$ and $DyCo_2Si_2$. *Journal of Physics: Condensed Matter*, 12:7455–7462, 2000.

[33] P. Schobinger-Papamantellos, K.H.J. Buschow, C. Ritter, and L. Keller. The magnetic phase diagram of the $HoCo_2X_2$ (X=Ge, Si) and $DyCo_2Ge_2$ compounds by neutron diffraction. *Journal of Magnetism and Magnetic Materials*, 264:130–141, 2003.

[34] G. André, P. Thuéry, M. Pinot, A. Oleś, and A. Szytuł. Magnetic structure of $TbCo_2B_2$. *Solid State Communications*, 80:239–241, 1991.

[35] J.M. Barandiaran, D. Gignoux, D. Schmitt, J.C. Gomez-sal, J. Rodriguez Fernandez, P. Chieux, and J. Schweizer. Magnetic properties and magnetic structure of $GdNi_2Si_2$ and $GdCu_2Si_2$ compounds. *Journal of Magnetism and Magnetic Materials*, 73:233–239, 1988.

[36] E.G. Gerasimov, P.B. Terentev, A.F. Gubkin, H.E. Fischer, D.I. Gorbunov, and N.V. Mushnikov. Easy-plane magnetic anisotropy in layered $GdMn_2Si_2$ compound with easy-axis magnetocrystalline anisotropy. *Journal of Alloys and Compounds*, 818:152902, 2020.

[37] W. Good, J. Kim, A.I. Goldman, D. Wemeille, P.C. Canfield, C. Cunningham, Z. Islam, J.C. Lang, G. Srajer, and I.R. Fisher. Magnetic structure of $GdCo_2Ge_2$. *Physical Review B*, 71:224427, 2005.